ACS APPLIED ENERGY MATERIALS

www.acsaem.org Article

Stability Enhancement of High-Performance Inverted Polymer Solar Cells Using ZnO Electron Interfacial Layer Deposited by Intermittent Spray Pyrolysis Approach

Enas Moustafa, José G. Sánchez, Lluis F. Marsal,* and Josep Pallarès*

Cite This: *ACS Appl. Energy Mater.* 2021, 4, 4099−4111 Read Online

ACCESS | Metrics & More | Article Recommendations | Supporting Information

ABSTRACT: In this research work, for the first time, stable high-performance inverted polymer solar cells (iPSCs) have been fabricated utilizing facile and low-cost intermittent spray pyrolysis (SP) technique to deposit transparent thin films of zinc oxide (ZnO) as electron interfacial transporting layer (ETL). The performed iPSCs have the structure of ITO/ZnO/PBDTTT-EFT:$PC_{70}BM$/V_2O_5/Ag. The thickness diversity of the ETL layer was adjusted by varying the concentration of the ZnO precursor solution, while fixed thicknesses were fabricated for the other layers in the iPSCs. Moreover, the influence of the deposition techniques on the interface roughness, performance, and stability of the devices has been detected and discussed. By increasing the concentration of the ZnO precursor solution as well as the number of spraying running cycles, the thickness and roughness of the ZnO film increase. The highest power conversion efficiency (10%) of the fresh iPSCs with ZnO-SP was obtained by using a ZnO-precursor solution concentration of 1:4 in ethanol with 7 spraying running cycles. This efficiency is almost the same as the iPSCs fabricated ZnO-ETL by the laboratory-scale spin coating (SC) technique that was used as a reference. Furthermore, it was interesting to observe that the stability of the devices intermittently sprayed by ZnO-SP was higher than the controlled reference ones that were fabricated by ZnO-SC. Hence, deep insight studies have been carried out for the fresh and degraded iPSCs using dark current−voltage characteristics and impedance spectroscopy measurements to investigate the electrical parameters for the ZnO film obtained by the SP and SC techniques. The results indicated that the interface roughness between the ZnO and the active layers plays an important role in enhancing light trapping and the light absorbance inside the cell which increases the generated electric current as well as the stability of the devices.

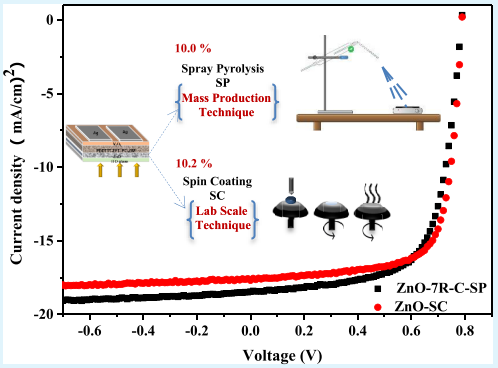

KEYWORDS: *polymer solar cells, spray pyrolysis, thin film deposition techniques, interfacial layers, film morphology, stability of organic solar cells*

1. INTRODUCTION

There is an urgent need to speed up moving on the development of renewable energy technologies in order to cover the shortages in energy demands nowadays along with reducing the CO_2 emission.[1] Accordingly, performing applications that can utilize the sunlight in terms of harvesting clean and renewable energy without burning the fossil fuels is an extremely attractive and essential approach. Photovoltaics or titled solar cells have been addressed as one of the most remarkable renewable energy technologies in the field of renewable solar energy.[2] The reason behind that is no greenhouse gas emission or any other gaseous pollutants are produced during the operation. Currently, polymer solar cells (PSCs) used for harnessing solar energy based on thin film organic materials get great attention due to their lightweight, high flexibility, low manufacturing cost, and short energy payback time as well as facile conjugation with other products and applications.[3,4] The efficiency of polymer solar cells has been dramatically increased from 6% to 18% during a period of less than one decade.[5−10] PSCs have been started with a single active layer, then a donor−acceptor bilayer followed by planar heterojunction, and a breakthrough to the bulk heterojunction (BHJ) which greatly improves the charge separation mechanism.[4,5,11,12] BHJ polymer solar cells were initially fabricated using a conventional structure of the conjugated p-type polymer semiconductor (electron donor) and n-type fullerene derivatives (electron acceptor) sandwiched between the transparent conducting oxide (TCO) anode, mostly indium tin oxide (ITO) that collects the holes and the low work function metal cathode (e.g., Al or Ca), which collects the electrons.[7,13] Unfortunately, this conventional structure

Received: February 12, 2021
Accepted: March 23, 2021
Published: April 5, 2021

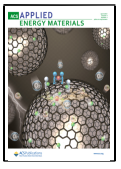

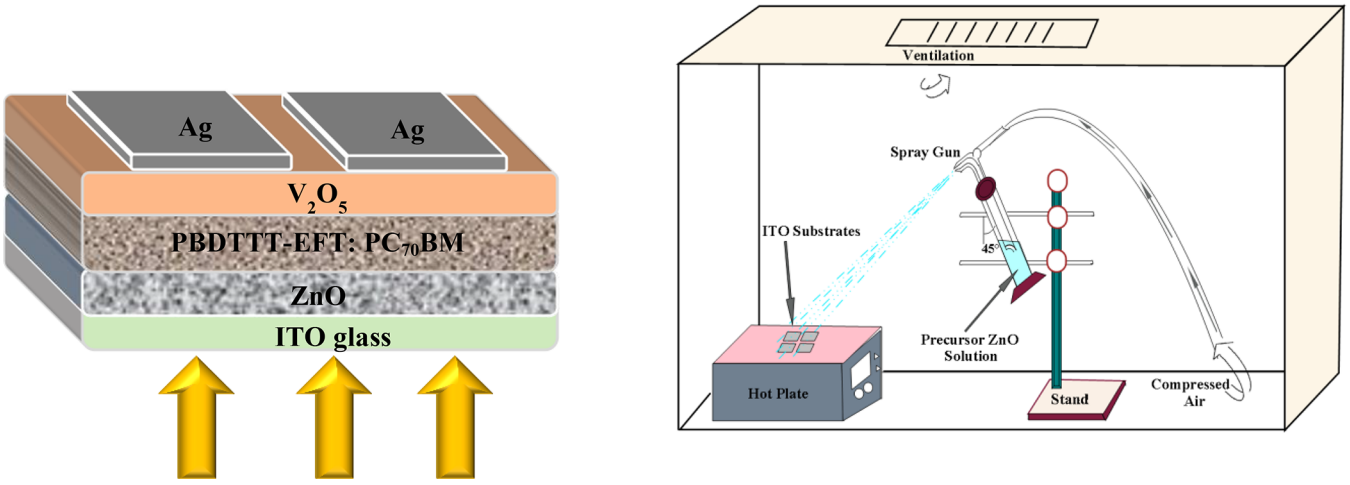

Figure 1. (a) Schematic illustration of the fabricated iPSCs structure, (b) Schematic diagram of the spray pyrolysis (SP) technique setup for ZnO-ETL thin film deposition.

suffers from rapid degradation due to the use of poly(3,4-ethylenedioxythiophene):poly(styrenesulfonate) (PEDOT:PSS) as an anode buffer layer, which is hygroscopic and acidic.[14] To overcome this potential problem and prevent the corrosion between the ITO and the PEDOT:PSS, polymer solar cells with an inverted structure (iPSCs) have been designed with air stable and high work function metal (e.g., Ag, Au) to collect holes, whereas ITO collects the generated electrons.[15,16] In this approach with regard to the iPSCs structure, there are two extra impeded layers with the purpose of enhancing the charge transfer during the cell operation and getting better performance of the iPSCs.[12,17−19] One is a transparent layer that is introduced between the ITO, and the active layer is named the electron-transporting layer (ETL). The other is located between the metal electrode and the active layer called the hole-transporting layer (HTL). However, the stability of the polymer solar cells is still an important issue to investigate the origin of the degradation processes that occurred and the mechanisms of the intrinsic or extrinsic degradation leads to device instability.[20−22] Most of the literature pointed to overcoming the extrinsic instability by the encapsulation to prevent the degradation due to the humidity and oxygen.[23] The other side of the intrinsic degradation was studied by using different interfacial layers and thin film materials.[20] In addition, understanding the degradation mechanism due to intrinsic instability of the solar cell's materials as well the impact of interfaces is important to avoid the main reason for this sort of degradation.[20,23] In the iPSCs, the type of the electron-transporting layer is one of the important factors that limit the performance of the devices. Commonly used ETLs in iPSCs are titanium dioxide (TiO_2), zinc oxide (ZnO), and poly[(9,9-bis(3-(*N*,*N*-dimethylamino)propyl)-2,7-fluorene)-*alt*-2,7-(9,9 dioctylfluorene)] (PFN).[18,23,24] ZnO thin film has been figured as one of the most promising oxide materials due to its high chemical stability and electrical properties. Also, it plays a virtual role in the optoelectronic applications as a metal oxide semiconductor that is alternative to TiO_2 such as perovskite, dye synthesized, thin film solar cells, photodetectors, and transistors.[16,25−30]

Moreover, in the iPSCs, thin film ZnO is used as ETL and a hole blocking layer as well because of its high electron mobility and transparency. In addition, ZnO films are simply synthesized by several chemical methods as well as controlling the morphology during the preparation and the deposition techniques are adaptable.[15,16,25,27,29]

Despite the importance of the materials used as ETL, the deposition techniques consider an essential factor because it controls the film morphology in addition to the interface roughness between the layers, which has a direct effect on the overall behavior and performance of the iPSCs.[31−33] Different thin film deposition techniques have been used for the fabrication of iPSCs such as roll to roll,[34] inkjet printing,[35] spin coating (SC),[18,36] and spray pyrolysis (SP) techniques.[37,38] The spray pyrolysis technique is one of the most economic techniques that has many superior advantages. It is a very simple thin film deposition technique that does not require any vacuum condition at any stage. That is a tremendously vital factor that allows the process to scale-up for industrial applications.[39−41] Furthermore, it is a cost-effective technique (especially regarding to the equipment costs), easy to control the deposition parameters, and a reproducible thin film deposition technique.[39,40] Moreover, the SP technique has the ability of fabricating the film by different compositions that enables preparing films with gradients through the film thickness, which is highly effective for the optical applications.[41,42]

In this research work, iPSCs have been fabricated on the basis of the optically active semiconducting polymer poly[4,8-bis(5-(2-ethylhexyl)thiophen-2-yl)benzo[1,2-*b*:4,5-*b*]dithiophene-*co*-3-fluorothieno[3,4*b*]thiophene-2-carboxylate] (PBDTTT-EFT) that blended with $PC_{70}BM$ to compose the active layer. A thin film of vanadium oxide (V_2O_5) has been used as HTL followed by silver (Ag) as a metal contact. Several studies have been reported on the fabrication of thin film ZnO ETL with SP technique in polymer solar cells.[43,44] However, currently, there are no reports of performed iPSCs using the SP technique to achieve high power conversion efficiency with the structure of ITO/ZnO/PBDTTT-EFT:$PC_{70}BM$/V_2O_5/Ag. Consequently, it is important to mention that our ZnO-ETL has been deposited using spray pyrolysis thin film deposition technique with the intermittent approach. That gave the niche of producing high ZnO film quality along with retaining the high performance and stability of the fabricated iPSCs. In parallel with the iPSCs fabricated by the SP, a laboratory-scale spin coating technique has been used to fabricate ZnO-ETL as a controlled reference iPSCs. Furthermore, different ZnO precursor solution concen-

https://doi.org/10.1021/acsaem.1c00455
ACS Appl. Energy Mater. 2021, 4, 4099−4111

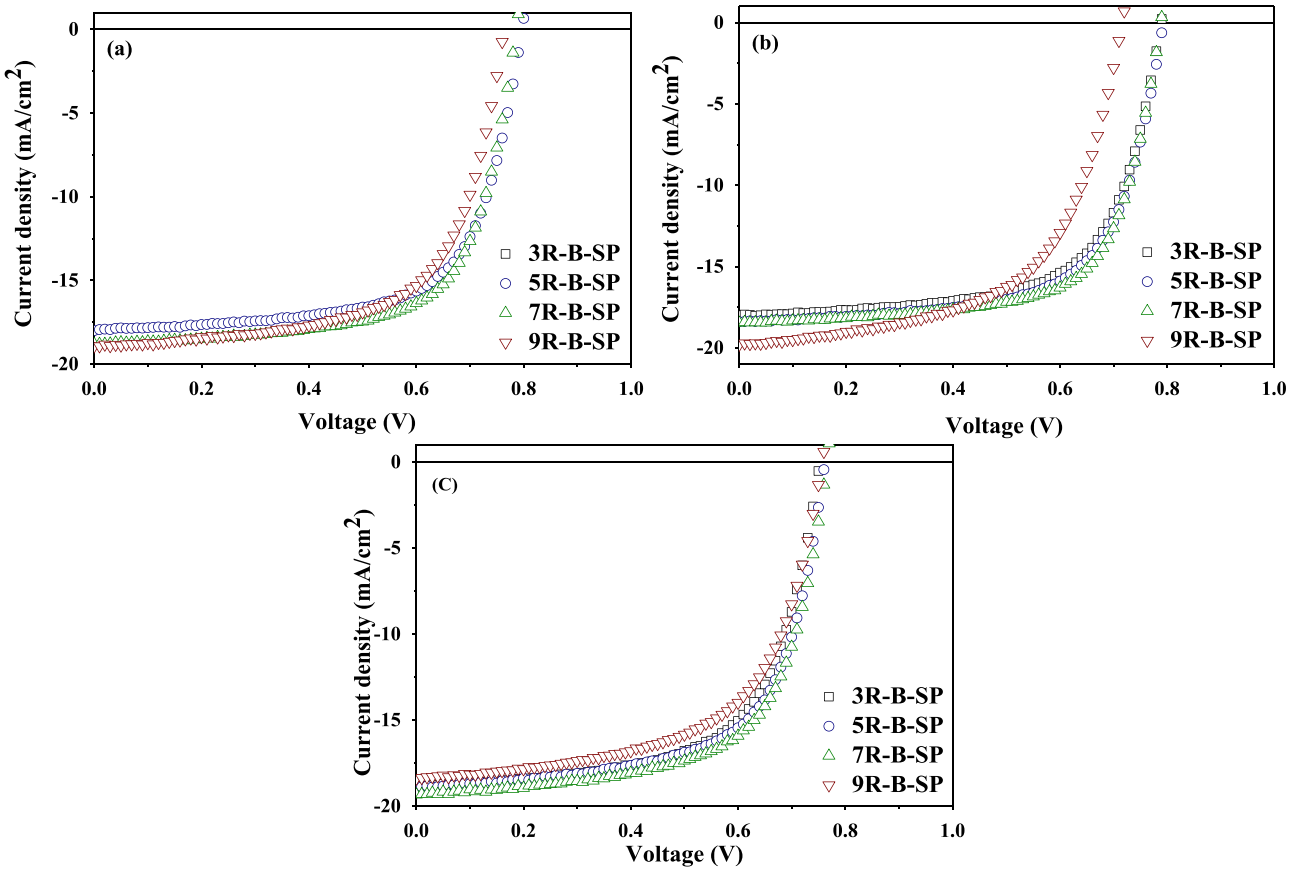

Figure 2. $J-V$ characteristic curves under illumination of the iPSCs fabricated by ZnO-ETL SP technique at running cycles of 3R, 5R, 7R, and 9R with ZnO precursor concentrations of (a) B(1:6)-ZnO-SP, (b) C(1:4)-ZnO-SP, and (c) D(1:2)-ZnO-SP.

trations and various spraying parameters have been investigated and optimized to perform efficient and stable iPSCs.

2. EXPERIMENTAL PROCEDURES

This section describes the materials used, the synthesis procedures, and the characterization tools used during the fabrication of iPSCs based on a structure of ITO/ZnO/PBDTTT-EFT:C_{70}BM/V_2O_5/Ag as shown in Figure 1a.

2.1. Materials. The TCO used was indium tin oxide patterned glass substrate with a resistivity of 10 Ω·sq^{-1} purchased from PsiOTec Ltd. For synthesizing the ZnO-ETL precursor solution, zinc acetate dihydrate (99.999%, A-Aldrich), 2-methoxyethanol (99.9%, Sigma-Aldrich), and ethanolamine 99.5% (A-Aldrich) were provided. The donor polymer PBDTTT-EFT and the fullerene acceptor $PC_{70}BM$ were supplied from One-Material Inc. and Solenne BV, respectively. V_2O_5 used as HTL was delivered from Sigma-Aldrich with 99.999% purity as well as the Ag, from Testbourne Ltd.

2.2. Device Fabrication. In the beginning, ITOs have been carefully cleaned with detergent and water, subsequent 10 min ultrasonicated in acetone, methanol, and isopropanol and then dried by nitrogen flow and placed in the oven at 100 °C for 10 min. Followed by UV−ozone treatment for 20 min to remove any organic residue as well as activating the ITO surface. The ZnO precursor solution was synthesized by dissolving 150 mg of zinc acetate dihydrate in 1 mL of 2-methoxyethanol and then added 30 μL of ethanolamine solution. Then, the mixture was left for 1 h under vigorous stirring at 70 °C. The prepared ZnO solution was diluted by methanol 1:1 (v/v) ratio to obtain the stock solution. In the case of fabricating the reference solar cells, ZnO stock solution was spin coated on the top of the precleaned ITO at 3000 rpm for 30 s and then left for 1 h annealing at 200 °C,[35] while, for the SP technique, the synthesized stock solution was diluted with ethanol and then sprayed over the preheated ITOs at 350 °C, and the deposited films were left to annealed for 1 h. Three different concentration ratios of ZnO solution have been prepared, B samples with 1:6 (v/v) ratio, C samples with 1:4 (v/v) ratio, and D samples with 1:2 (v/v) ratio. It is worth mentioning that our approach of spraying procedure is different than the conventional continues spraying one to avoid the accumulation that might produce defects in the film and as consequence affect the performance of the devices.[43,45,46] In our method, the spraying process was intermittently where each spraying running cycle (1R) takes 7 s of direct solution spraying and 3 s hold and then starting the next cycle following the same procedures. Moreover, each concentration of the mentioned samples (B, C, and D) was used to fabricate the ZnO layers by applying different numbers of running cycles (3R, 5R, 7R, and 9R). The spray pyrolysis setup used for depositing the ZnO-ETL schematically illustrated in Figure 1b. This experimental setup consists of a glass spraying gun, a temperature-controlled hot plate, and a stand holder that flexibly changes the distance between the spraying gun and the samples on the surface of the hot plate. The spraying gun consists of a double-nozzle sprayer that coaxially conjugated with quartz and a capillary tube inside. The glass spraying gun was attached to the stand holder during the deposition process. The ZnO prepared precursor solution inlet through the capillary tube together with the quartz tube that passes the compressed air as a carrier gas in order to spray the ZnO precursor solution on the top of the preheated ITOs. The distance between the gun and the ITO substrate was adjusted to cover the entire deposited surfaces.

The active blend solution consisted in a 25 mg/mL solution of PBDTTT-EFT:$PC_{70}BM$ with 1:1.5 (w/w) ratio, in chlorobenzene:-DIO (97:3 (%, v/v)). Then the blend is stirred and heated at 40 °C for 18 h. The prepared solution was left for 48 h for aging and then filtered and spun over the ZnO film at 750 rpm for 30 s to obtain a thickness of 100 nm.[47] Lastly, the samples were introduced to a vacuum chamber to thermally evaporate V_2O_5 followed by Ag films under high-vacuum conditions ($\leq 1 \times 10^{-6}$ mbar) to obtain thicknesses of 4 and 100 nm,

https://doi.org/10.1021/acsaem.1c00455
ACS Appl. Energy Mater. 2021, 4, 4099−4111

Table 1. Performance Parameters for B-ZnO-SP, C-ZnO-SP, and D-ZnO-SP iPSCs Fabricated by Spray Pyrolysis (SP) Technique with Running Cycles of 3R, 5R, 7R, and 9R and the ZnO-SC Reference[a]

	V_{OC} (V)	J_{SC} (mA·cm^{-2})	FF (%)	PCE (%)	R_S (Ω·cm^2)	R_{SH} (Ω·cm^2)
B (1:6)						
9R	0.75 ± 0.01	18.51 ± 0.43	63.61 ± 0.39	9.00 ± 0.19	1.96 ± 0.15	610 ± 22
best	0.76	18.94	64.00	9.19	2.11	582
7R	0.78 ± 0.01	18.14 ± 0.64	67.00 ± 0.20	9.73 ± 0.24	3.04 ± 0.12	610 ± 6
best	0.79	18.78	67.20	9.97	2.47	616
5R	0.79 ± 0.01	17.46 ± 0.54	65.41 ± 0.59	9.23 ± 0.26	2.43 ± 0.45	664 ± 7
best	0.80	18.00	66.00	9.49	2.88	671
3R	0.78 ± 0.01	16.69 ± 0.55	65.86 ± 0.24	8.61 ± 1.28	3.00 ± 0.38	642 ± 13
best	0.79	17.24	66.10	8.89	3.08	655
C (1:4)						
9R	0.71 ± 0.01	19.37 ± 0.27	58.38 ± 0.62	8.11 ± 20	3.21 ± 0.25	298 ± 12
best	0.72	19.64	59.00	8.31	2.79	300
7R	0.79 ± 0.01	18.04 ± 0.42	68.04 ± 0.57	9.82 ± 0.18	2.80 ± 0.20	734 ± 20
best	0.79	18.46	68.61	10.00	2.83	720
5R	0.78 ± 0.01	17.79 ± 0.60	66.57 ± 0.46	9.48 ± 0.12	2.96 ± 0.23	604 ± 7
best	0.79	18.39	67.03	9.60	2.89	611
3R	0.78 ± 0.01	17.54 ± 0.45	65.86 ± 0.46	8.78 ± 0.54	3.40 ± 0.31	758 ± 16
best	0.79	17.99	66.32	9.32	2.98	764
D (1:2)						
9R	0.75 ± 0.01	17.94 ± 0.45	59.65 ± 0.35	8.21 ± 0.19	2.46 ± 0.19	400 ± 17
best	0.76	18.39	60.00	8.40	2.67	417
7R	0.75 ± 0.01	18.70 ± 0.32	63.80 ± 0.40	9.15 ± 0.15	2.23 ± 0.60	490 ± 28
best	0.76	19.02	64.20	9.30	2.00	499
5R	0.74 ± 0.02	18.86 ± 0.20	63.29 ± 0.71	9.08 ± 0.21	1.87 ± 0.24	564 ± 26
best	0.76	19.06	64.00	9.29	2.07	590
3R	0.75 ± 0.02	18.74 ± 0.23	62.91 ± 0.209	8.95 ± 0.09	2.63 ± 0.19	511 ± 17
best	0.75	18.97	63.20	9.04	2.11	524
ZnO-SC						
	0.79 ± 0.01	17.45 ± 0.28	72.60 ± 0.40	10.00 ± 0.20	1.90 ± 0.13	1129 ± 13
best	0.79	17.69	73.00	10.19	1.03	1140

[a]The average parameters were calculated from a minimum 8 fabricated cells of each.

respectively. The evaporation process was performed using a shadow mask to design a cell with an area of 0.09 cm^2. Considering that the entire fabrication process (after depositing the ZnO films) has proceeded inside the glovebox under a controlled nitrogen atmosphere.

2.3. Device Characterizations. Atomic force microscope (AFM) was utilized to investigate the surface topography by tapping mode for detecting the surface roughness of the prepared ZnO films using spin coating and spray pyrolysis techniques. The thicknesses of the prepared ZnO films were measured by the surface profilometer (AMBIOS TECHNOLOGY-XP-1). The transmittance and reflectance spectra were performed at room temperature using PerkinElmer Lambda 950 UV/vis/NIR spectrometer with an integrating sphere. Current density−voltage (J−V) characteristics curves and parameters of the fabricated iPSCs have been investigated with a Keithley 2400 source-measure unit at room temperature under illumination using a solar simulator (Abet Technology model 11000 class type A, Xenon arc) and dark conditions. Calibration for the solar simulator intensity was operated with a Fraunhofer certified photovoltaic cell to yield a 100 mW/cm^2 and AM1.5 spectrum. In addition, a mask with a well-defined area has been attached to the sample holder in order to specify the effective area for accurate measurement. External quantum efficiency (EQE) measurements were performed with the wavelength range from 300 to 800 nm using Lasing, S.A. (IPCE-DC, LS1109-232) and a Newport 2936-R power-meter unit system. Impedance spectroscopy (IS) measurements were carried out at different applied bias voltages (0.0 V, 0.5 V, and V_{OC}) and an AC signal with 50 mV amplitude at frequency range 5 Hz to 1 MHz, utilizing the same AM1.5 illumination conditions with HP-4192A impedance analyzer.

3. RESULTS AND DISCUSSION

In this research work, the effect of different concentrations of ZnO precursor solutions and the spraying conditions by intermittent SP technique on the performance and the stability of iPSCs have been investigated. In addition, the high-efficiency iPSCs fabricated with the optimized SP-deposition conditions have been compared with the state-of-the-art reference cells fabricated by the laboratory-scale SC technique (sample A, ZnO-SC).

3.1. Optimization of ZnO Film Deposited by Spray Pyrolysis Technique. In order to optimize the thin ZnO film by SP technique, three different concentrations of ZnO solution, B (1:6), C (1:4), and D (1:2) were sprayed with four different numbers of running cycles (3R, 5R, 7R, and 9R) as described in Experimental Section. The fabricated iPSCs were identified as B-ZnO-SP, C-ZnO-SP, and D-ZnO-SP, respectively. The performance parameters of the mentioned iPSCs fabricated have been extracted from the illustrated current density−voltage characteristic curves represented in Figure 2. Table 1 demonstrates the performance parameters for B-ZnO-SP, C-ZnO-SP, and D-ZnO-SP iPSCs. It has been observed that the entire fabricated iPSCs have fairly the same V_{OC}. Moreover, the performance of the solar cells improved as the concentration of ZnO-precursor solution increased from B to C but decreased in the D concentration. Besides, as the number of running cycles increased from 3R to 7R, the performance of the iPSCs was

https://doi.org/10.1021/acsaem.1c00455
ACS Appl. Energy Mater. 2021, 4, 4099−4111

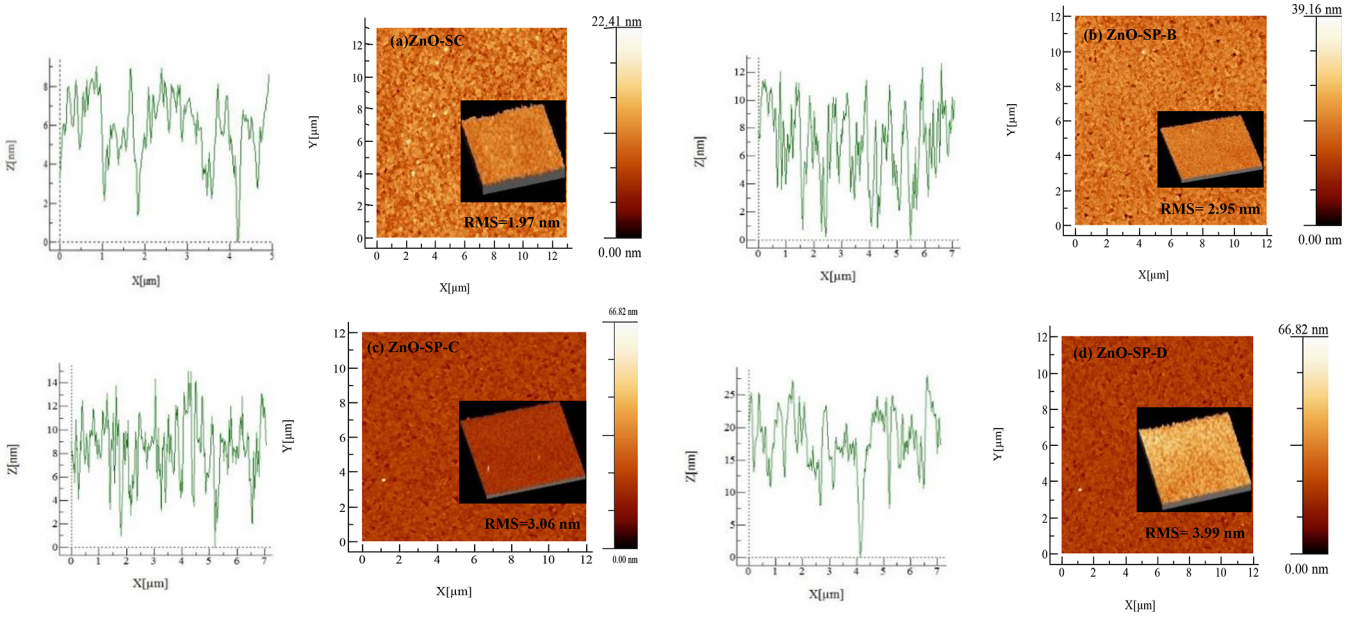

Figure 3. AFM topographical images of the ZnO films deposited by SC (a) and 7R-SP cells of B (b), C (c), and D (d) concentrations.

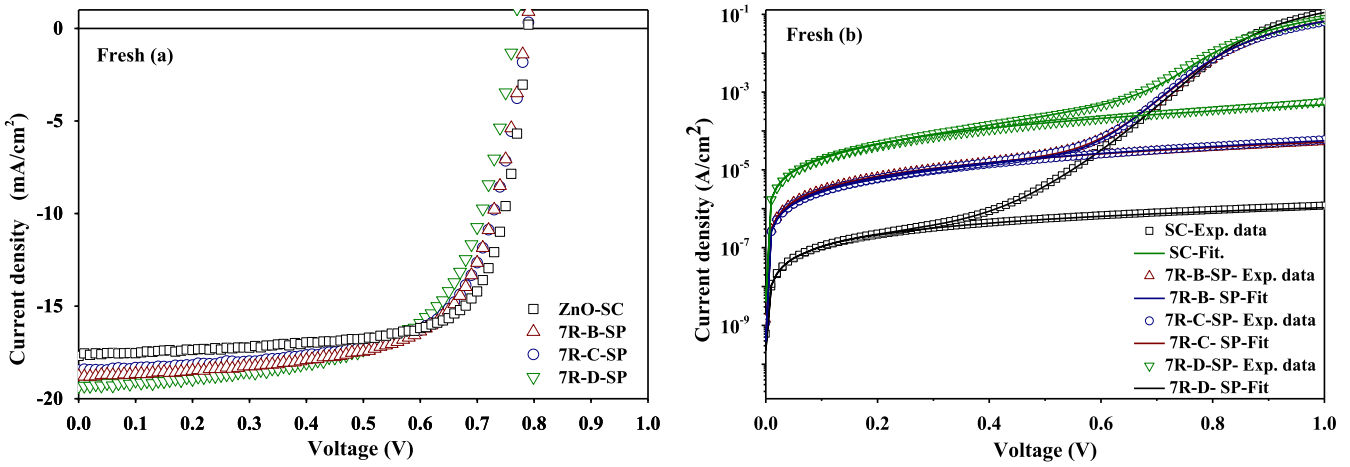

Figure 4. *J*−*V* characteristic curves of 7R-B-SP, 7R-C-SP, and 7R-D-SP fabricated by SP and the reference cell ZnO-SC fabricated by laboratory-scale SC (a) under illumination conditions (AM 1.5) and (b) at dark condition (symbols for experimental data and the lines for the fitting).

enhanced except for 9R, which decreased again as illustrated in Figure S1a.

For B-ZnO-SP devices fabricated by 7R-SP technique, the measured values of open circuit voltage (V_{OC}), current density (J_{SC}), fill factor (FF), series resistance (R_S), shunt resistance (R_{SH}), and power conversion efficiency (PCE) were 0.79 V, 18.78 mA/cm^2, 67.20%, 2.47 Ω·cm^2, 616 Ω·cm^2, and 9.97%, respectively. While for the C-ZnO-SP cells performed with 7R, the V_{OC}, J_{SC}, FF, R_S, R_{SH}, and PCE were 0.79 V, 18.46 mA/cm^2, 68.61%, 2.83 Ω·cm^2, 720 Ω·cm^2, and 10.00%, respectively. The D-ZnO-SP devices with 7R were obtained V_{OC} = 0.76 V, J_{SC} = 19.02 mA/cm^2, FF = 64.20%, R_S = 2.00 Ω·cm^2, R_{SH} = 499 Ω·cm^2, and PCE of 9.30%. The lower performance of sample D-ZnO-SP might be due to the highest concentration of the ZnO precursor solution D, as well as high numbers of running cycles (9R) deposited which increase the thickness along with decreasing R_{SH} that affected negatively on the performance of the devices. Consequently, at B, C, and D concentrations, the iPSCs prepared by the 7R-SP have followed the same trend of showing higher performance among those prepared by 3R, 5R, and 9R. In addition, the devices with C concentration showed the highest performance as illustrated in Figure S1b.

On the basis of the exhibited results, the iPSCs with 7R for B, C, and D concentrations have been selected to be compared with the reference-controlled devices fabricated by the lab-scale SC technique (Sample A: ZnO-SC) because they have obtained the best performance among 3R, 5R, and 9R iPSCs.

3.2. Study and Analysis of the iPSCs with ZnO-ETL Deposited by SC and the Optimum of 7R-SP Techniques.

The following section explains in detail the effects of the concentration of ZnO precursor solutions (B, C, and D) sprayed by 7R-SP intermittently on the film formation and the interfacial roughness as well as the performance of the iPSCs, besides comparison with the standard reference ZnO-SC iPSCs. As illustrated in Figure 3, AFM images show the surface roughness topographical profile for the prepared ZnO films using SC and SP techniques. The estimated root-mean-square (RMS) surface roughness values of ZnO films were 1.97, 2.95, 3.06, and 3.99 nm for SC, B-7R-SP, C-7R-SP, and D-7R-SP, respectively. The average thicknesses of ZnO-film were 30, 20, 25, and 50 nm for

https://doi.org/10.1021/acsaem.1c00455
ACS Appl. Energy Mater. 2021, 4, 4099−4111

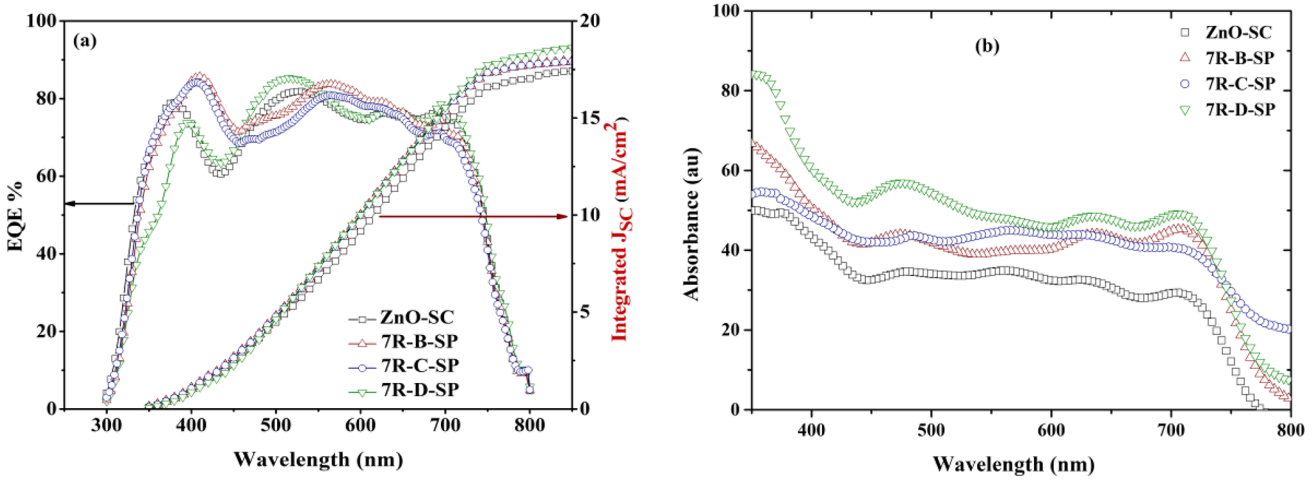

Figure 5. (a) EQE spectra (left) and the integrated short circuit current (right), (b) UV−visible optical characteristics of the ITO/ZnO/active layer structure of the 7R-B-SP, 7R-C-SP and 7R-D-SP iPSCs fabricated by SP technique and the reference cell ZnO-SC fabricated by SC.

ZnO-SC, B-7R-SP, C-7R-SP, and D-7R-SP, respectively. Through these studies, it has been investigated that the ZnO films prepared by the SP technique possess higher surface roughness values than those deposited by the SC technique. This indicates that the coating method itself has an impact on the film morphology and roughness where the SC technique usually provides a smooth and uniform film, while SP technique is known as a randomly spraying method which produces more rough film than the SC technique.[37,48]

In addition, regarding the ZnO films sprayed by the SP, as the concentration of the prepared ZnO solution increases, the thickness along with the roughness increased.

Figure 4a illustrates the illuminated $J-V$ measurements of the iPSCs performed by 7R-SP with B, C, and D concentrations along with the ZnO-SC-controlled reference cells. The detailed comparison of the performance parameters is shown in Table 1 and Supporting Information Figure S2. Despite the best efficiency values being obtained for the reference ZnO-SC iPSCs, these devices have the lowest short circuit current values. This can be due to the difference in the thickness and surface roughness of the ZnO film sprayed by SP, which proves that there is a dependence on the device's performance on the thickness and roughness of the sprayed ZnO films. Moreover, the lowest performance of D-7R-SP iPSCs can be attributed to the interface mismatch as a consequence of higher concentration and ZnO-surface roughness.

Figure 4b presents the $J-V$ characteristic curve under dark conditions for the iPSCs with 7R-SP of B, C, and D concentrations and the ZnO-SC devices. This figure shows the experimental data (symbols) and the fitting model values (line) of the fabricated devices using a two diodes equivalent model as illustrated in Figure S3. It is important to mention that not only the usual series and shunt resistances are included but also a space charge limiting current (SCLC) element is needed to properly fit the experimental fresh ZnO-SP data at the reverse and low forward voltages because of the high-leakage current density (J_{rev}). The fitting values are shown in Table S1. We found that all of the samples showed a similar exponential mechanism with n_1 around 1.25 at medium forward voltages and saturation current density values of $0.6 < J_{01}$ (10^{-13} A/cm^2) < 5.8. In addition, the J_{rev} for D-7R-ZnO-SP samples is higher than those of B-7R-ZnO-SP and C-7R-ZnO-SP devices. This confirms the effect of surface roughness of the film because D-7R-ZnO-SP devices have the highest surface roughness of the ZnO film, which consequently, affected the D-7R-SP cells' performance by having the lowest R_{SH} that plays an effective role in decreasing the PCE of the fabricated devices. This attitude can be ascribed to the created trapping sites due to the formation of aggregated ZnO particles on the film surface related to the high concentration of the ZnO−D solution.[49−52]

In fact, ZnO-SC iPSCs have shown a higher performance but a lower J_{SC} and J_{rev}, while D-7R-SP iPSCs showed a lower performance but a higher J_{SC} and J_{rev}. On one hand, the reduction of V_{OC} and FF as R_{SH} decreases can be found elsewhere.[53,54] On the other hand, the enhancement of J_{SC} as R_{SH} decreases cannot be explained using electrical parameters but optically in the following section.

Figure 5a displays the EQE spectra for the fabricated devices, which have a similar range of absorption, but a slight difference in the intensities and the shape between the spectra that is probably due to a difference in light reflection properties of the ZnO-ETL layers in the devices because of the roughness and thickness variations. The calculated J_{SC} from the integration of the EQE spectra for the SC-ZnO, B-7R-SP, C-7R-SP, and D-7R-SP iPSCs were 17.57, 18.43, 18.01, and 18.82 mA/cm^2, respectively, which agreed with the measured ones obtained from the $J-V$ characteristics under illumination shown in Table 1. The achieved results showed an increase in the J_{SC} for the cells prepared by ZnO-SP more than as prepared by the ZnO-SC technique. This observation indicates the higher absorption of photons as confirmed by UV−vis analysis for the calculated absorbance spectra in Figure 5b for the ITO/ZnO/active layer structure. The spray-coated ZnO devices showed higher absorbance than the ZnO-SC ones. In addition, Figure S4a demonstrates that the transmission for the ITO/ZnO-SP/active layer structures was lower than the ITO/ZnO-SC/active layer structures, which indicates that the active layer in the SP devices absorbed more light than the ZnO-SC fabricated devices. It is worth mentioning that D-7R-SP iPSCs exhibit the highest J_{SC} and the highest ZnO film roughness. That is in good agreement with the observed phenomena of increasing the absorbance and the light trapping inside the solar cells by increasing the surface roughness.[33,55,56] The reflectance depends on the surface roughness for each layer as well as affects the interfaces related to the light trapping that takes place inside the cell.[33,55] Accordingly, the reflectance decreases as the roughness

https://doi.org/10.1021/acsaem.1c00455
ACS Appl. Energy Mater. 2021, 4, 4099−4111

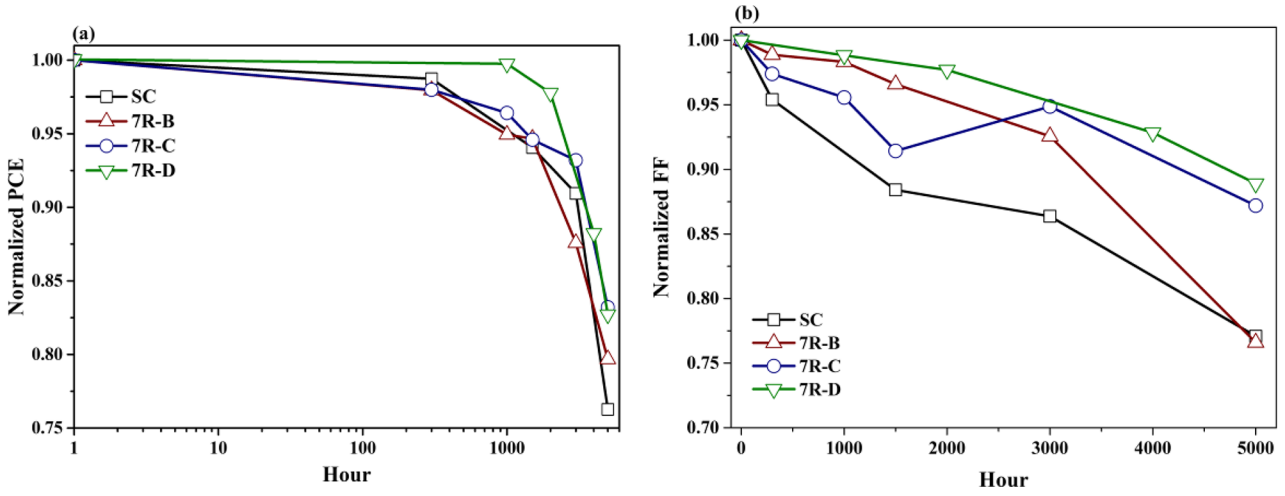

Figure 6. (a) Normalized power conversion efficiency of the iPSCs devices regarding their initial values as a function of time T_{80} (after 5000 h) and (b) normalized FF curve over T_{80} degradation time.

increases, which is indicated by increasing the absorbance as a result of the effect of light trapping that occurred inside the cell,[3,33,56,57] as shown in Figure S4b. Moreover, the observed EQE results confirm the obtained transmittance measurements presented in Figure S4a.

Consequently, the observed lower transmittance and reflectance of the ZnO-7R-SP samples than the ZnO-SC ones were due to the higher interface roughness between the ZnO layer and the active layer. This interface roughness assisted the light trapping inside the cells to obtain higher light absorbance and enhances the current generation J_{SC}, from which it has been monitored that the lowest reflectance produces the best light trapping for higher interface roughness D-7R-SP samples fabricated by the SP technique.

3.3. Stability Study of ZnO-SC and Optimal ZnO-7R-SP iPSCs. The stability of the fabricated iPSCs has been investigated through a comparison between the performance behavior of ZnO-SC, B-7R-SP, C-7R-SP, and D-7R-SP iPSCs over time where the devices reached about 80% (T_{80}—after 5000 h) of their initial efficiencies (T_{100}—0 h). This is to study the influence of the ZnO-ETL deposited by SC and intermittent SP techniques along with the respective interface to the active layer on the stability of the fabricated devices, by varying only the fabrication conditions of the ZnO-ETL between the devices that enabled specifying the degradation effect related to the ETL interface in the devices. The mentioned fabricated iPSCs were exposed to light during the $J-V$ measurement and afterward returned inside the glovebox in dark during the entire investigation period in electronic grade 99.999% N_2 (H_2O < 0.1 ppm; O_2 < 0.1 ppm). From this comparison, it can be noticed that a decrease in the performance of the solar cells has occurred, as shown in Figure S5 and Table S2, where the experimental measurements and the correlated performance parameters of the fabricated iPSCs during the degradation process are presented, respectively.

Figure 6a shows the decay of the normalized PCE of the iPSCs fabricated by the 7R-SP and SC techniques after 5000 h (T_{80}). It depicted the T_{80} degradation for the ZnO-7R-SP iPSCs was slower than that of the ZnO-SC iPSCs, where the normalized PCE% for the fabricated ZnO-SC, B-7R-SP, C-7R-SP, and D-7R-SP iPSCs were 76.42%, 79.68%, 84.20%, and 82.72%, respectively. Consequently, it can be noticed that the PCE decay rate over time for the iPSCs fabricated using C-7R-SP was slower than that fabricated by ZnO-SC as well as the other concentrations by the SP technique. That might be attributed to the enhancement of the interfacial formed between the active layer and the sprayed ZnO layer. By evaluating the transient of the normalized performance parameters plotted in Figure S6, the V_{OC} of entire devices have been kept almost the same during the degradation test for 5000 h, which might represent the stability of the active layer as it was kept inside the glovebox.[21,22] In addition, we can notice that J_{SC} has changed in a different trend as it first enhanced then decreased slowly. Also, the values of R_{SH} decreased for the iPSCs fabricated by the SC technique, while there was a fluctuation between increasing and decreasing for the SP-7R iPSCs. But the R_S was obviously increased for the whole fabricated iPSCs. Furthermore, there was a clear decrease in the FF which might be due to increasing the R_S of the devices over time as clarified from the normalized FF curve of the degraded iPSCs in Figure 6b and Figure S6b. These curves confirmed that the decrease in the FF is the main factor that reduces the PCE over time, indicating the presence of electrodes or interfacial layers degradation.[21] In addition, it should be emphasized that the decay of the performance parameters related to the ZnO-SC iPSCs were faster than the 7R-SP iPSCs. Accordingly, the iPSCs fabricated using ZnO-SP showed higher intrinsic stability more than those fabricated by ZnO-SC.

Furthermore, these obtained results are in good agreement with the dark $J-V$ characteristics, as shown in Figure S7. The figure showed a clear increase in the leakage current upon degradation for the entire devices as confirmed by the fitting parameters for the T_{80} and T_{90} (devices reached about 90% from the initial value) summarized in Table S3 and Table S4, respectively. Also, these results have the same behavior observed in the previous works that report long lifetimes of devices exposed only under nitrogen environment.[58,59]

3.4. Impedance Spectroscopy Insight Analysis for Studying the Effect of ZnO-Interfacial Deposited Layer by SC and 7R-SP Techniques of the Fresh and Degraded iPSCs. In this part, a deep study has been performed for the T_{100} fresh and T_{80} degraded ZnO-SC and ZnO-7R-SP iPSCs using impedance spectroscopy. It is a powerful method for analyzing the bulk and interface properties in solar cells besides diagnosing degradation effects in organic solar cells.[60,61]

The change in trap emission can be tracked through capacitance measurements since it is known that semiconductor

https://doi.org/10.1021/acsaem.1c00455
ACS Appl. Energy Mater. 2021, 4, 4099−4111

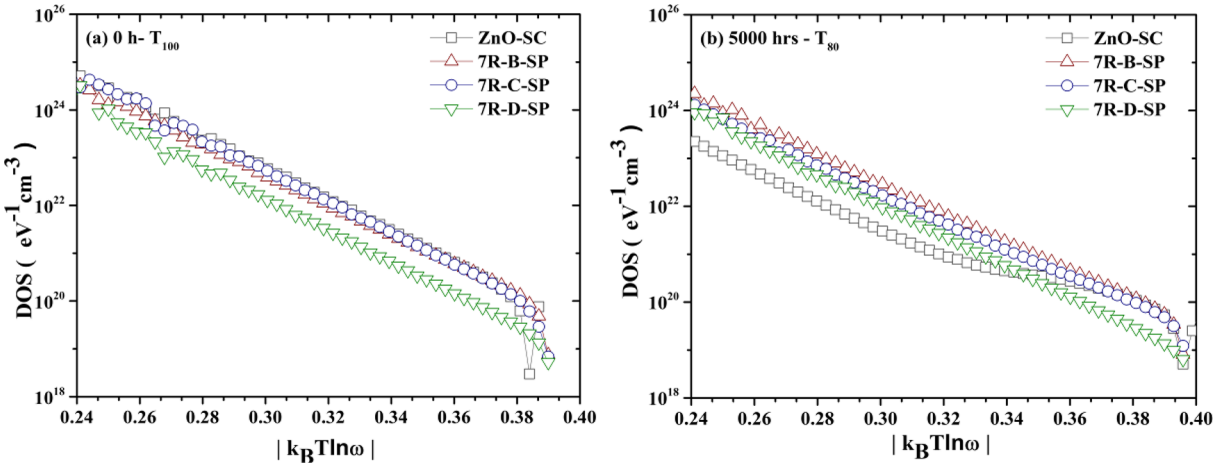

Figure 7. Density of state (DOS) as a function of energy of ZnO-SC, B-7R-SP, C-7R-SP, and D-7R-SP iPSCs under AM1.5 illumination: (a) freshly prepared iPSCs and (b) iPSCs after 5000 h in N_2 atmosphere.

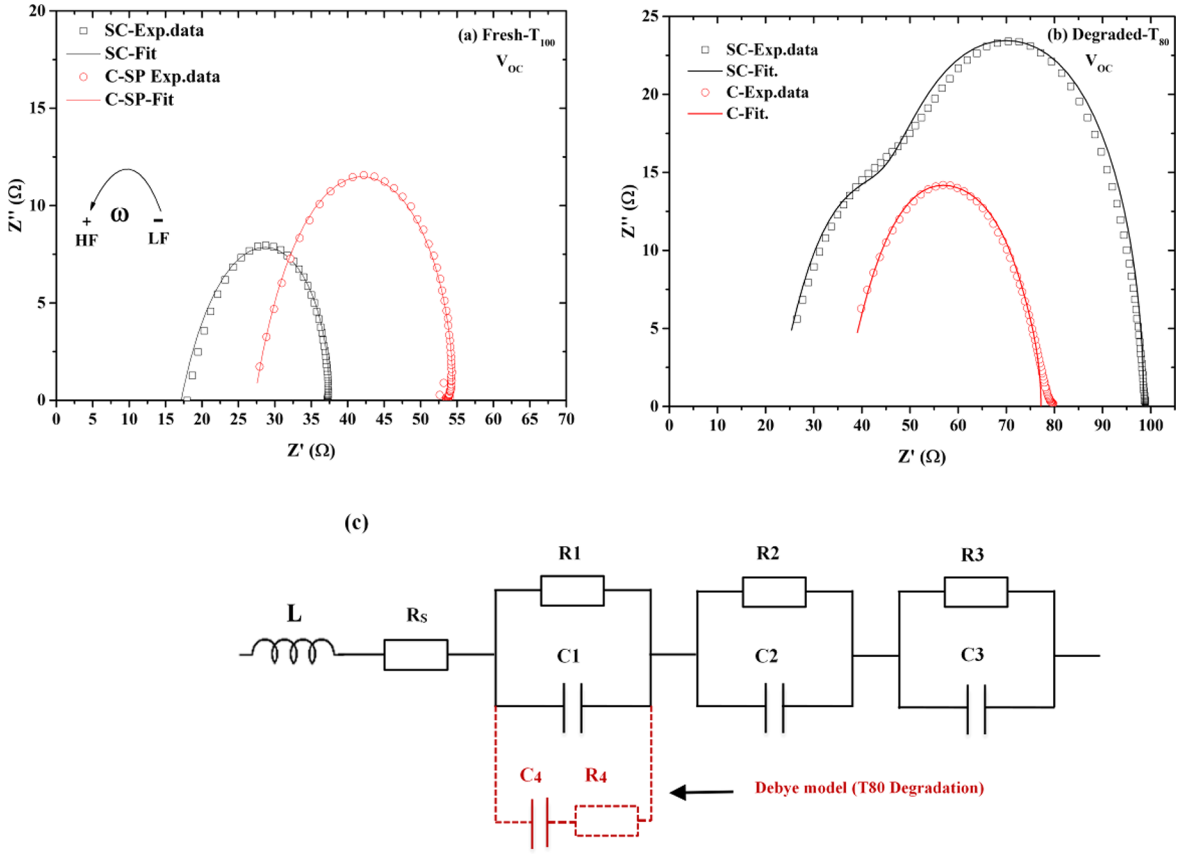

Figure 8. Impedance spectra measured under illumination (IS-AM1.5) for ZnO-SC and C-7R-SP iPSCs at V_{OC} (a) for the T_{100} freshly prepared iPSCs and (b) for the degraded iPSCs after 5000 h (T_{80}). Using symbols for the experimental data and the fitting results in solid lines by applying the equivalent circuit model, (c) 3RC solid black lines for the fresh prepared iPSCs and the added dashed red lines for the T_{80} degraded iPSCs following the Debye model.

devices have a depletion region that exhibits parallel plate-like capacitance, named the depletion capacitance.[62,63] Thus, IS has been used for measuring the capacitance−frequency to calculate the density of state that has been operated for polymer:fullerene solar cells.[20,63,64] The DOS at a given energy level, E_ω, can be estimated assuming that the variation of the capacitance of the device with the frequency is related to the trapping and release of charge by shallow trap sites in the band gap close to the Fermi energy level as follows:[20,65]

$$\mathrm{DOS}(E_\omega)_{\mathrm{traps}} = -\frac{V_{\mathrm{Bi}}\omega}{tqTk_{\mathrm{B}}}\frac{\partial C}{\partial \omega} \quad (1)$$

where C is the measured capacitance, V_{Bi} is the built-in voltage (assuming that $V_{\mathrm{Bi}} = V_{\mathrm{OC}}$), ω is the angular frequency, t is the layer thickness, k_{B} is the Boltzmann constant, q is the electron charge, and T is room temperature (300 K).

https://doi.org/10.1021/acsaem.1c00455
ACS Appl. Energy Mater. 2021, 4, 4099−4111

To convert the dependence of the DOS from the angular momentum into energy dependence, the following equation has been applied:

$$(E_\omega)_{\text{traps}} = k_B T \ln\left(\frac{2\beta N}{\omega}\right) = E_O - k_B T \ln \omega \quad (2)$$

where β is the cross-section and N is the effective density of state.[65,66] Since assuming that $2\beta N$ is independent of the frequency value, the change in its value is related to the shift in the DOS values on the energy scale, E_O. Regarding the freshly prepared devices, DOS values presented in Figure 7a show a single-exponential trap distribution for all of the samples. In addition, the same slope values were obtained which defines the same trap activation energy and carrier response.[67] However, the main difference was obtained in the D-7R-SP samples with the lowest DOS values for a given frequency. We can explain this result using eq 2, as a shift in the E_O value due to the increase of the βN value. As a consequence, it is expected to have lower energy as a result of higher traps located in the iPSCs which confirm the low performance of the D-7R-SP samples.

In Figure 7b, we found that the T_{80} degraded ZnO-SC devices create more trapping sites than the ZnO-SP devices. In addition, it can be noticed that deep traps states have been observed only for the devices fabricated by the ZnO-SC technique due to the degradation process. On the other hand, the devices fabricated by the ZnO-SP technique showed only shallow traps of tail states. Furthermore, by comparing the energy shift values of the T_{100} fresh and the T_{80} degraded samples shown in Figure S8, we obtained that the degraded ZnO-SC devices have almost five times trapping sites more than the fresh ones. While the T_{80} degraded ZnO-SP devices showed less than double the trapping of the tail state only. Accordingly, after 5000 h of degradation, it can be said that the ZnO-SP iPSCs have a higher stability than ZnO-SC devices. That also has been confirmed by the mentioned $J-V$ degradation tests.

As an alternative way for an insight analysis to manifest the difference in the performance of the fabricated iPSCs due to the interface roughness effect, a comparison between the real and imaginary impedance measurements has been carried out for the best cells' performance of C-7R-SP and the controlled reference cell ZnO-SC has been inspected. Figure 8a shows a typical semicircle behavior of Nyquist plot for the fresh ZnO-SC and C-7R-SP iPSCs, with a bias voltage of V_{OC}. It has been observed that at a given frequency the Cole−Cole plot of the ZnO-SC devices has lower series resistance as well a smaller arc radius size than the C-7R-SP devices. This might explain the higher performance of the T_{100} fresh ZnO-SC iPSCs. On the other hand, Figure 8b illustrates the arc behavior with some deviation from the typical shape due to the T_{80} degradation, where a second arc appeared at a high frequency more clearly in the ZnO-SC devices in addition to the higher arc radius than the C-7R-SP devices. This might confirm the faster degradation behavior related to the ZnO-SC than the C-7R-SP samples shown in the previous characterizations. Moreover, these behaviors have been observed also in the Cole−Cole plot at a bias voltage of 0.5 V illustrated in Figure S9.

Figure 8c demonstrates the electrical equivalent circuit used to fit the experimental $Z'-Z''$ data. The components used to fit the plots with one arc, fresh iPSCs, are shown in black solid lines, whereas the additional components used to fit the second arc that appeared at high frequency, T_{80} degraded iPSC, are shown in red dashed lines. This circuit model consists of distributed resistors, R, which refer to the resistance of electrons transportation in each layer where R1, R2, and R3 are with regard to V_2O_5, ZnO, and the blend layers, respectively. In addition, C refers to the geometrical capacitance values of each layer, proving a parallel association of resistor and capacitor for three resistor/capacitor elements in series (3RC). R_S represents the series resistance from the ITO layer as well due to the interface between the ITO and the ETL,[23,68,69] and L is the added inductor to fit the data at high frequency. It is important to mention that the model composed of an extra impeded R4C4 in series which attached in parallel to R1C1 that followed the Debye model[69] to explain the effect of the degradation takes place in the iPSCs over time. This model considers the presence of a single type of trap created in one layer. Also, the parameter values of each layer were fitted simultaneously.

To gain further insight into the obtained fitted data summarized in Table S5, it can be exhibited not only that the fitting capacitance values for each layer for both samples fabricated by SP and SC techniques are similar but also that they are in good agreement with the theoretical values shown in Table S6. Also, it can be concluded that at V_{OC} the IS data were controlled by the geometrical capacitances related to the metal−insulator−metal (MIM) model providing the presence of fully depleted layers.[70]

Regarding the resistance values obtained from the fitting, several differences were found for the ZnO-SC vs C-7R-SP iPSCs. But the main difference results from the R_S element as the ZnO film deposited by the SP technique has higher values than that produced from the ZnO film deposited by the SC technique. This explained the arc of the fresh T_{100} C-7R-SP plot that appears at a lower frequency as well as higher arc radius than the ZnO-SC shown in Figure 8a, where the R_S values for the fresh ZnO-SC were around 7 Ω, which might be referred to as the ITO film resistance, while, for the C-7R-SP, the R_S values were around 12 Ω, which could be attributed to the ITO film resistance in addition to the interface resistance between the ZnO film deposited by SP and the ITO. This observed result is correlated with the Bode plot at V_{OC} and 0.5 V in Figure S10. This might be related to the higher interface roughness between the ITO and the ZnO layer coated by SP. In addition, it was in good agreement with the R_S evaluated by the $J-V$ characterization as shown in Table 1. Moreover, during the fabrication of the iPSCs and the degradation test discussed before, the V_{OC} of entire devices almost did not show severe changes, so that the active layer did not affect by the deposition operation of the ZnO layer, so that it can be assumed that the main effect was related to the ZnO/ITO interface, because ITO was the main layer exposed to the high temperature of 350 °C during the SP deposition, which might affect its interface resistance with the ZnO layer. This means that the increment of the resistance was not related to the layer itself, even if it has been deposited by different techniques, but it was related to the interface effect.

Furthermore, Table S7 presents the extracted charge time (τ) values for the fabricated iPSCs at V_{OC} and 0.5 V, where, at V_{OC} for the freshly prepared iPSCs, the τ of the ZnO-SC (1.1×10^{-6} s) was a bit smaller than the ones for the C-7R-SP (1.3×10^{-6} s), which also correlated with the previously obtained results providing much higher performance of the fresh ZnO-SC devices. The same trend of the results has been observed for the iPSCs at 0.5 V.

Regarding the additional arc observed in Figure 8b at high frequency for the T_{80} degraded iPSCs, specially ZnO-SC devices, it has been successfully fitted by the extra R4C4 circuit

https://doi.org/10.1021/acsaem.1c00455
ACS Appl. Energy Mater. 2021, 4, 4099−4111

using the Debye model.[70] On one side, it is essential to note that the extra C4 value of the V_2O_5 layer of both ZnO-SC and C-7R-SP were almost the same giving the highest layer capacitance in the devices which limits the performance for both devices due to the presence of a single type of traps that has created in the V_2O_5 layer during the degradation process. On the other side, this second arc could be explained by the great increase in the resistance of the V_2O_5 layer in the T_{80} degraded ZnO-SC iPSCs (53.0 Ω) in comparison with the C-7R-SP cells (17.8 Ω) as showed in Table S5. Moreover, Figure S11 illustrates the Bode plot for the ZnO-SC and C-7R-SP iPSCs at V_{OC} and 0.5 V for T_{80} degraded iPSCs. This plot confirms the higher resistance observed by the ZnO-SC devices after T_{80} degradation which results in decreasing the performance of the device along with the stability. In addition, the τ for the degraded ZnO-SC iPSCs (7.4×10^{-6} s) was higher than the ones of C-7R-SP (6.5×10^{-6} s) at V_{OC} as shown in Table S7. As it was limited by the V_2O_5 layer because of the highest R and C values, the same considered behavior observed at 0.5 V for the T_{80} degraded iPSCs. That might be the same reason for the increasing arc size for T_{80}-degraded ZnO-SC devices more than the arc obtained for the C-7R-SP devices in Figure 8b. This could be attributed to the deposition mechanism using the intermittent SP approach. Where tiny spray droplets quickly dried on a hot substrate (350 °C) which immediately evaporates on top of the ITO. Furthermore, the holding time of this approach avoids the accumulation or retaining of any solvents or moisture inside the ZnO layer during the deposition. That might minimize the layer degradation and consequently the contacted layers and the entire device. In addition, the spraying technique with high substrate temperature helps solution adhesion and bonding to itself and to the substrate to obtain a high-quality layer. That might explain the better stability of the fabricated devices using the SP technique.[37] Furthermore, the same behavior of the Nyquist and the Bode plots has been observed for the B-7R-SP and D-7R-SP samples as shown in Figure S12 and the summarized fitting parameters listed in Table S8.

Finally, it can be noticed that the C and τ were quite equal for both freshly fabricated iPSCs by SC and SP techniques. However, after the degradation test, the iPSCs fabricated by the C-7R-SP technique showed lower τ and lower decay of the performance, which indicated the enhancement of the stability of the devices that also was confirmed by the $J-V$ and DOS analysis.

4. CONCLUSION

The effect of different concentrations for the ZnO precursor solutions B, C, and D to deposit a thin film of the ZnO-ETL using intermittent spray pyrolysis approach have been investigated on the performance and the stability of the fabricated iPSCs. The films fabricated by the intermittent SP techniques demonstrated more surface roughness than that deposited by the SC technique. In the case of the iPSCs fabricated using the ZnO-SP technique, the results demonstrated that the 7R-SP have shown higher iPSCs' performance more than the others. Moreover, C-7R-SP devices showed higher J_{SC} more than that fabricated by the laboratory-scale ZnO-SC technique and fairly similar performance achieving devices with the same V_{OC} (0.79 V) as well efficiency of 10%. It was noticeable that the main difference between the fabricated iPSCs by ZnO-SC and C-7R-SP obtained from the interface roughness effect between the ITO and the ZnO deposited film. The good side was regarding the active layer side, that being a textured surface enhances the light trapping inside the solar cell which increases the absorbance of the incident light and generates higher J_{SC}. In addition, this proper interface contact with the active layer enhances the overall stability for the ZnO-SP iPSCs. While the negative side was the effect of the interface between the ZnO sprayed layer and the ITO that increases the R_S. However, the rate of degradation of the iPSCs fabricated by the ZnO-SP technique was slower than the iPSCs synthesized by the ZnO-SC technique. It is important to consider that the main advantages for the C-7R-SP iPSCs were not only higher J_{SC} and longer stability but also the ability to fabricate the ZnO-ETL using the SP technique with maintaining the high performance of the iPSCs.

Moreover, for the leakage current $J-V$ dark characteristics assuming SCLC was the appropriate model to evaluate the losses that resulted from the trap sites. In addition, impedance spectroscopy provided a detailed mechanism regarding the interface effect obtained which clarifies the main difference that occurred due to the performed deposition techniques. Furthermore, not only the exponential tail density of states can be calculated for fresh and degraded samples but also the electrical equivalent circuit analysis using the 3RC and Debye models. These models presented a simple way to diagnose the loss mechanisms and investigate degradation mechanisms and stability issues in the fabricated devices.

Hence, the investigated results point out that the deposition techniques have a vital role that affects the film formation as well as the performance and stability of the devices. Taking these facts into account leads to the next step of improving the interface between the ZnO layer and the ITO to perform lower R_S, which might enhance the device stability and performance. Lastly, the intermittent spray pyrolysis approach is a powerful, low-cost, simple, and reproducible technique. It is promising for integrating the iPSCs to the industrial scale by easily attaching it with the roll to roll and other mass production techniques.

■ ASSOCIATED CONTENT

Supporting Information

The Supporting Information is available free of charge at https://pubs.acs.org/doi/10.1021/acsaem.1c00455.

Performance parameters details of T_{100} and T_{80}; fabricated iPSCs using SC and SP techniques; fresh and degraded devices' behavior explanation; IS and DOS equivalent electrical circuits to fit experimental dark $J-V$ measurements (PDF)

■ AUTHOR INFORMATION

Corresponding Authors

Lluis F. Marsal − *Department of Electrical Electronic Engineering and Automatic, Universitat Rovira i Virgili, Tarragona 43007, Spain;* orcid.org/0000-0002-5976-1408; Email: Lluis.Marsal@urv.cat

Josep Pallarès − *Department of Electrical Electronic Engineering and Automatic, Universitat Rovira i Virgili, Tarragona 43007, Spain;* orcid.org/0000-0001-7221-5383; Email: josep.pallares@urv.cat

Authors

Enas Moustafa − *Department of Electrical Electronic Engineering and Automatic, Universitat Rovira i Virgili, Tarragona 43007, Spain;* orcid.org/0000-0003-4190-8456

José G. Sánchez − *The Institute of Chemical Research of Catalonia-The Barcelona Institute of Science and Technology (ICIQ-BIST), Tarragona 43007, Spain*

Complete contact information is available at: https://pubs.acs.org/10.1021/acsaem.1c00455

Notes

The authors declare no competing financial interest.

■ ACKNOWLEDGMENTS

The work of E.M. was financially supported by the AGAUR for receiving the fund with Grant No. 2019 FI_B01102. In addition, this work was supported by the Spanish Ministerio de Ciencia, Innovacion y Universidades (MICINN/FEDER) Grant No. RTI2018-094040-B-I00 and by the Agency for Management of University and Research Grants (AGAUR) Reference No. 2017-SGR-1527.

■ ABBREVIATIONS

DOS = density of state
EQE = external quantum efficiency
FF = fill factor
iPSCs = inverted polymer solar cells
IS = impedance spectroscopy
J_{rev} = leakage current
J_{SC} = current density
$J-V$ = current density−voltage
open circuit voltage = V_{OC}
PCE = power conversion efficiency
R = spraying running cycles
R_S = series resistance
R_{SH} = shunt resistance
SC = spin coating
SCLC = space charge limiting current
SP = spray pyrolysis

■ REFERENCES

(1) Singh, S. P.; Islam, A. Intelligent Materials for Solar Cells. *Adv. OptoElectron.* **2012**, *2012*, 919728.
(2) Servaites, J. D.; Ratner, M. A.; Marks, T. J. Organic Solar Cells: A New Look at Traditional Models. *Energy Environ. Sci.* **2011**, *4*, 4410−4422.
(3) Haberlin, H. *Photovoltaics System Design And Practice*; John Wiley & Sons, 2012; Vol. *1*. DOI: 10.1002/9781119976998
(4) Krebs, F. C. Fabrication and Processing of Polymer Solar Cells: A Review of Printing and Coating Techniques. *Sol. Energy Mater. Sol. Cells* **2009**, *93* (4), 394−412.
(5) Lin, Y.; Adilbekova, B.; Firdaus, Y.; Yengel, E.; Faber, H.; Sajjad, M.; Zheng, X.; Yarali, E.; Seitkhan, A.; Bakr, O. M.; El-Labban, A.; Schwingenschlögl, U.; Tung, V.; McCulloch, I.; Laquai, F.; Anthopoulos, T. D. 17% Efficient Organic Solar Cells Based on Liquid Exfoliated WS_2 as a Replacement for PEDOT:PSS. *Adv. Mater.* **2019**, *31* (46), 1902965.
(6) Ma, L.; Zhang, S.; Wang, J.; Xu, Y.; Hou, J. Recent Advances in Non-Fullerene Organic Solar Cells: From Lab to Fab. *Chem. Commun.* **2020**, *56* (92), 14337−14352.
(7) Lu, L.; Zheng, T.; Wu, Q.; Schneider, A. M.; Zhao, D.; Yu, L. Recent Advances in Bulk Heterojunction Polymer Solar Cells. *Chem. Rev.* **2015**, *115* (23), 12666−12731.
(8) Cui, Y.; Yao, H.; Zhang, J.; Zhang, T.; Wang, Y.; Hong, L.; Xian, K.; Xu, B.; Zhang, S.; Peng, J.; Wei, Z.; Gao, F.; Hou, J. Over 16% Efficiency Organic Photovoltaic Cells Enabled by a Chlorinated Acceptor with Increased Open-Circuit Voltages. *Nat. Commun.* **2019**, *10* (1), 2515.
(9) Zhan, L.; Li, S.; Lau, T. K.; Cui, Y.; Lu, X.; Shi, M.; Li, C. Z.; Li, H.; Hou, J.; Chen, H. Over 17% Efficiency Ternary Organic Solar Cells Enabled by Two Non-Fullerene Acceptors Working in an Alloy-like Model. *Energy Environ. Sci.* **2020**, *13* (2), 635−645.
(10) Cui, Y.; Yao, H.; Zhang, J.; Xian, K.; Zhang, T.; Hong, L.; Wang, Y.; Xu, Y.; Ma, K.; An, C.; He, C.; Wei, Z.; Gao, F.; Hou, J. Single-Junction Organic Photovoltaic Cells with Approaching 18% Efficiency. *Adv. Mater.* **2020**, *32* (19), 1908205.
(11) Abdulrazzaq, O. A.; Saini, V.; Bourdo, S.; Dervishi, E.; Biris, A. S. Organic Solar Cells: A Review of Materials, Limitations, and Possibilities for Improvement. *Part. Sci. Technol.* **2013**, *31* (5), 427−442.
(12) Li, G.; Zhu, R.; Yang, Y. Polymer Solar Cells. *Nat. Photonics* **2012**, *6* (3), 153−161.
(13) Norrman, K.; Gevorgyan, S. A.; Krebs, F. C. Water-Induced Degradation of Polymer Solar Cells Studied by $H_2{}^{18}O$ Labeling. *ACS Appl. Mater. Interfaces* **2009**, *1* (1), 102−112.
(14) Kawano, K.; Pacios, R.; Poplavskyy, D.; Nelson, J.; Bradley, D. D. C.; Durrant, J. R. Degradation of Organic Solar Cells Due to Air Exposure. *Sol. Energy Mater. Sol. Cells* **2006**, *90* (20), 3520−3530.
(15) Sun, Y.; Seo, J. H.; Takacs, C. J.; Seifter, J.; Heeger, A. J. Inverted Polymer Solar Cells Integrated with a Low-Temperature-Annealed Sol-Gel-Derived ZnO Film as an Electron Transport Layer. *Adv. Mater.* **2011**, *23* (14), 1679−1683.
(16) White, M. S.; Olson, D. C.; Shaheen, S. E.; Kopidakis, N.; Ginley, D. S. Inverted Bulk-Heterojunction Organic Photovoltaic Device Using a Solution-Derived ZnO Underlayer. *Appl. Phys. Lett.* **2006**, *89* (14), 143517.
(17) He, Z.; Zhong, C.; Su, S.; Xu, M.; Wu, H.; Cao, Y. Enhanced Power-Conversion Efficiency in Polymer Solar Cells Using an Inverted Device Structure. *Nat. Photonics* **2012**, *6* (9), 591−595.
(18) Balderrama, V. S.; Sánchez, J. G.; Lastra, G.; Cambarau, W.; Arias, S.; Pallarès, J.; Palomares, E.; Estrada, M.; Marsal, L. F. High-Efficiency Organic Solar Cells Based on a Halide Salt and Polyfluorene Polymer with a High Alignment-Level of the Cathode Selective Contact. *J. Mater. Chem. A* **2018**, *6* (45), 22534−22544.
(19) Mayer, A. C.; Scully, S. R.; Hardin, B. E.; Rowell, M. W.; McGehee, M. D. Polymer-Based Solar Cells. *Mater. Today* **2007**, *10* (11), 28−33.
(20) Ecker, B.; Nolasco, J. C.; Pallarés, J.; Marsal, L. F.; Posdorfer, J.; Parisi, J.; Von Hauff, E. Degradation Effects Related to the Hole Transport Layer in Organic Solar Cells. *Adv. Funct. Mater.* **2011**, *21* (14), 2705−2711.
(21) Grossiord, N.; Kroon, J. M.; Andriessen, R.; Blom, P. W. M. Degradation Mechanisms in Organic Photovoltaic Devices. *Org. Electron.* **2012**, *13* (3), 432−456.
(22) Jørgensen, M.; Norrman, K.; Krebs, F. C. Stability/Degradation of Polymer Solar Cells. *Sol. Energy Mater. Sol. Cells* **2008**, *92* (7), 686−714.
(23) Osorio, E.; Sánchez, J. G.; Acquaroli, L. N.; Pacio, M.; Ferré-Borrull, J.; Pallarès, J.; Marsal, L. F. Degradation Analysis of Encapsulated and Nonencapsulated TiO_2/PTB7:$PC_{70}BM$/V_2O_5 Solar Cells under Ambient Conditions via Impedance Spectroscopy. *ACS Omega* **2017**, *2* (7), 3091−3097.
(24) Li, T.; Chen, Z.; Wang, Y.; Tu, J.; Deng, X.; Li, Q.; Li, Z. Materials for Interfaces in Organic Solar Cells and Photodetectors. *ACS Appl. Mater. Interfaces* **2020**, *12* (3), 3301−3326.
(25) Wang, H.; Cao, S.; Yang, B.; Li, H.; Wang, M.; Hu, X.; Sun, K.; Zang, Z. NH_4Cl-Modified ZnO for High-Performance $CsPbIBr_2$ Perovskite Solar Cells via Low-Temperature Process. *Sol. RRL* **2020**, *4* (1), 1900363.
(26) Cao, S.; Wang, H.; Li, H.; Chen, J.; Zang, Z. Critical Role of Interface Contact Modulation in Realizing Low-Temperature Fabrication of Efficient and Stable $CsPbIBr_2$ Perovskite Solar Cells. *Chem. Eng. J.* **2020**, *394*, 124903.
(27) Li, C.; Han, C.; Zhang, Y.; Zang, Z.; Wang, M.; Tang, X.; Du, J. Enhanced Photoresponse of Self-Powered Perovskite Photodetector Based on ZnO Nanoparticles Decorated $CsPbBr_3$ Films. *Sol. Energy Mater. Sol. Cells* **2017**, *172*, 341−346.

(28) Cho, J.; Hwang, S.; Ko, D. H.; Chung, S. Transparent ZnO Thin-Film Deposition by Spray Pyrolysis for High-Performance Metal-Oxide Field-Effect Transistors. *Materials* **2019**, *12* (20), 3423.
(29) Wang, H.; Zhang, P.; Zang, Z. High Performance $CsPbBr_3$ Quantum Dots Photodetectors by Using Zinc Oxide Nanorods Arrays as an Electron-Transport Layer. *Appl. Phys. Lett.* **2020**, *116* (16), 162103.
(30) Zang, Z. Efficiency Enhancement of ZnO/Cu_2O Solar Cells with Well Oriented and Micrometer Grain Sized Cu_2O Films. *Appl. Phys. Lett.* **2018**, *112* (4), 042106.
(31) Amratisha, K.; Ponchai, J.; Kaewurai, P.; Pansa-Ngat, P.; Pinsuwan, K.; Kumnorkaew, P.; Ruankham, P.; Kanjanaboos, P. Layer-by-Layer Spray Coating of a Stacked Perovskite Absorber for Perovskite Solar Cells with Better Performance and Stability under a Humid Environment. *Opt. Mater. Express* **2020**, *10* (7), 1497.
(32) Jehl, Z.; Bouttemy, M.; Lincot, D.; Guillemoles, J. F.; Gerard, I.; Etcheberry, A.; Voorwinden, G.; Powalla, M.; Naghavi, N. Insights on the Influence of Surface Roughness on Photovoltaic Properties of State of the Art Copper Indium Gallium Diselenide Thin Films Solar Cells. *J. Appl. Phys.* **2012**, *111* (11), 114509.
(33) Scholtz, L.; Ladanyi, L.; Mullerova, J. Influence of Surface Roughness on Optical Characteristics of Multilayer Solar Cells. *Adv. Electr. Electron. Eng.* **2015**, *12* (6), 631−638.
(34) Søndergaard, R.; Hösel, M.; Angmo, D.; Larsen-Olsen, T. T.; Krebs, F. C. Roll-to-Roll Fabrication of Polymer Solar Cells. *Mater. Today* **2012**, *15*, 36−49.
(35) Sánchez, J. G.; Balderrama, V. S.; Garduño, S. I.; Osorio, E.; Viterisi, A.; Estrada, M.; Ferré-Borrull, J.; Pallarès, J.; Marsal, L. F. Impact of Inkjet Printed ZnO Electron Transport Layer on the Characteristics of Polymer Solar Cells. *RSC Adv.* **2018**, *8* (24), 13094−13102.
(36) Torimtubun, A. A. A.; Sánchez, J. G.; Pallarès, J.; Marsal, L. F. A Cathode Interface Engineering Approach for the Comprehensive Study of Indoor Performance Enhancement in Organic Photovoltaics. *Sustain. Energy Fuels* **2020**, *4* (7), 3378−3387.
(37) Eslamian, M. Spray-on Thin Film PV Solar Cells: Advances, Potentials and Challenges. *Coatings* **2014**, *4* (1), 60−84.
(38) Aziz, F.; Ismail, A. F. Spray Coating Methods for Polymer Solar Cells Fabrication: A Review. *Mater. Sci. Semicond. Process.* **2015**, *39*, 416−425.
(39) Perednis, D.; Gauckler, L. J. Thin Film Deposition Using Spray Pyrolysis. *J. Electroceram.* **2005**, *14* (2), 103−111.
(40) Mooney, J. B.; Radding, S. B. Spray Pyrolysis Processing. *Annu. Rev. Mater. Sci.* **1982**, *12*, 81−101.
(41) Adamopoulos, G.; Bashir, A.; Wöbkenberg, P. H.; Bradley, D. D. C.; Anthopoulos, T. D. Electronic Properties of ZnO Field-Effect Transistors Fabricated by Spray Pyrolysis in Ambient Air. *Appl. Phys. Lett.* **2009**, *95* (13), 133507.
(42) Singh, D. V. K. Thin Film Deposition by Spray Pyroysis Techniques. *J. Emerg. Technol. Innov. Res. (JETIR)* **2017**, *4* (11), 910−918.
(43) Noh, Y. J.; Na, S. I.; Kim, S. S. Inverted Polymer Solar Cells Including ZnO Electron Transport Layer Fabricated by Facile Spray Pyrolysis. *Sol. Energy Mater. Sol. Cells* **2013**, *117*, 139−144.
(44) Cheng, J.; Hu, R.; Wang, Q.; Zhang, C.; Xie, Z.; Long, Z.; Yang, X.; Li, L. Substrate Temperature Effect on Charge Transport Performance of ZnO Electron Transport Layer Prepared by a Facile Ultrasonic Spray Pyrolysis in Polymer Solar Cells. *Int. J. Photoenergy* **2015**, *2015*, 201472.
(45) Lehraki, N.; Aida, M. S.; Abed, S.; Attaf, N.; Attaf, A.; Poulain, M. ZnO Thin Films Deposition by Spray Pyrolysis: Influence of Precursor Solution Properties. *Curr. Appl. Phys.* **2012**, *12* (5), 1283−1287.
(46) Ji, R.; Zheng, D.; Zhou, C.; Cheng, J.; Yu, J.; Li, L. Low-Temperature Preparation of Tungsten Oxide Anode Buffer Layer via Ultrasonic Spray Pyrolysis Method for Large-Area Organic Solar Cells. *Materials* **2017**, *10* (7), 820.
(47) Ramírez-Como, M.; Balderrama, V. S.; Sacramento, A.; Marsal, L. F.; Lastra, G.; Estrada, M. Fabrication and Characterization of Inverted Organic PTB7:$PC_{70}BM$ Solar Cells Using Hf-In-ZnO as Electron Transport Layer. *Sol. Energy* **2019**, *181*, 386−395.
(48) Prasada Rao, T.; Santhoshkumar, M. C. Effect of Thickness on Structural, Optical and Electrical Properties of Nanostructured ZnO Thin Films by Spray Pyrolysis. *Appl. Surf. Sci.* **2009**, *255* (8), 4579−4584.
(49) Pallarès, J.; Cabré, R.; Marsal, L. F.; Schropp, R. E. I. A Compact Equivalent Circuit for the Dark Current-Voltage Characteristics of Nonideal Solar Cells. *J. Appl. Phys.* **2006**, *100* (8), 084513−084515.
(50) Nolasco, J. C.; Cabré, R.; Ferré-Borrull, J.; Marsal, L. F.; Estrada, M.; Pallarès, J. Extraction of Poly (3-Hexylthiophene) (P3HT) Properties from Dark Current Voltage Characteristics in a P3HT/ n -Crystalline-Silicon Solar Cell. *J. Appl. Phys.* **2010**, *107* (4), 044505.
(51) Samiee, M.; Joshi, P.; Aidarkhanov, D.; Dalal, V. Measurement of Defect Densities and Urbach Energies of Tail States in PTB7 Solar Cells. *Appl. Phys. Lett.* **2014**, *105* (13), 133511.
(52) Peiró, A. M.; Ravirajan, P.; Govender, K.; Boyle, D. S.; O'Brien, P.; Bradley, D. D. C.; Nelson, J.; Durrant, J. R. The Effect of Zinc Oxide Nanostructure on the Performance of Hybrid Polymer/Zinc Oxide Solar Cells. *Proc. SPIE* **2005**, *5938*, 593819.
(53) Proctor, C. M.; Nguyen, T. Q. Effect of Leakage Current and Shunt Resistance on the Light Intensity Dependence of Organic Solar Cells. *Appl. Phys. Lett.* **2015**, *106* (8), 083301.
(54) Qi, B.; Wang, J. Fill Factor in Organic Solar Cells. *Phys. Chem. Chem. Phys.* **2013**, *15* (23), 8972−8982.
(55) Müller, J.; Rech, B.; Springer, J.; Vanecek, M. TCO and Light Trapping in Silicon Thin Film Solar Cells. *Sol. Energy* **2004**, *77* (6), 917−930.
(56) Krč, J.; Zeman, M.; Kluth, O.; Smole, F.; Topič, M. Effect of Surface Roughness of ZnO:Al Films on Light Scattering in Hydrogenated Amorphous Silicon Solar Cells. *Thin Solid Films* **2003**, *426* (1−2), 296−304.
(57) Sheng, X.; Broderick, L. Z.; Kimerling, L. C. Photonic Crystal Structures for Light Trapping in Thin-Film Si Solar Cells: Modeling, Process and Optimizations. *Opt. Commun.* **2014**, *314*, 41−47.
(58) Voroshazi, E.; Verreet, B.; Aernouts, T.; Heremans, P. Long-Term Operational Lifetime and Degradation Analysis of P3HT:PCBM Photovoltaic Cells. *Sol. Energy Mater. Sol. Cells* **2011**, *95* (5), 1303−1307.
(59) Vázquez, V. B. Fabrication of Bulk and Interdigitated Organic Solar Cells and Analysis of Degradation Mechanisms. Ph.D. Thesis, Rovira I Virgili University, Spain, 2014.
(60) Ecker, B.; Egelhaaf, H. J.; Steim, R.; Parisi, J.; Von Hauff, E. Understanding S-Shaped Current-Voltage Characteristics in Organic Solar Cells Containing a TiO x Interlayer with Impedance Spectroscopy and Equivalent Circuit Analysis. *J. Phys. Chem. C* **2012**, *116* (31), 16333−16337.
(61) Von Hauff, E. Impedance Spectroscopy for Emerging Photovoltaics. *J. Phys. Chem. C* **2019**, *123* (18), 11329−11346.
(62) Hegedus, S. S.; Fagen, E. A. Midgap States in A-Si:H and a-SiGe:H p-i-n Solar Cells and Schottky Junctions by Capacitance Techniques. *J. Appl. Phys.* **1992**, *71* (12), 5941−5951.
(63) Wang, S.; Kaienburg, P.; Klingebiel, B.; Schillings, D.; Kirchartz, T. Understanding Thermal Admittance Spectroscopy in Low-Mobility Semiconductors. *J. Phys. Chem. C* **2018**, *122* (18), 9795−9803.
(64) Reis, F. T.; Santos, L. F.; Bianchi, R. F.; Cunha, H. N.; Mencaraglia, D.; Faria, R. M. Application of Abrupt Cut-off Models in the Analysis of the Capacitance Spectra of Conjugated Polymer Devices. *Appl. Phys. A: Mater. Sci. Process.* **2009**, *96* (4), 909−914.
(65) Haneef, H. F.; Zeidell, A. M.; Jurchescu, O. D. Charge Carrier Traps in Organic Semiconductors: A Review on the Underlying Physics and Impact on Electronic Devices. *J. Mater. Chem. C* **2020**, *8* (3), 759−787.
(66) Walter, T.; Herberholz, R.; Müller, C.; Schock, H. W. Determination of Defect Distributions from Admittance Measurements and Application to $Cu(In,Ga)Se_2$ Based Heterojunctions. *J. Appl. Phys.* **1996**, *80* (8), 4411−4420.

https://doi.org/10.1021/acsaem.1c00455
ACS Appl. Energy Mater. 2021, 4, 4099−4111

(67) Carr, J. A.; Elshobaki, M.; Chaudhary, S. Deep Defects and the Attempt to Escape Frequency in Organic Photovoltaic Materials. *Appl. Phys. Lett.* **2015**, *107* (20), 203302.
(68) Garcia-Belmonte, G.; Munar, A.; Barea, E. M.; Bisquert, J.; Ugarte, I.; Pacios, R. Charge Carrier Mobility and Lifetime of Organic Bulk Heterojunctions Analyzed by Impedance Spectroscopy. *Org. Electron.* **2008**, *9* (5), 847−851.
(69) He, Z.; Huang, K.; Guo, C.; Jin, Z.; Hou, C. A Debye Dispersion Model of a Two-Layered Material. *AIP Adv.* **2019**, *9* (4), 045321.
(70) Schroeder, H. Poole-Frenkel-Effect as Dominating Current Mechanism in Thin Oxide Films - An Illusion?! *J. Appl. Phys.* **2015**, *117* (21), 215103.

https://doi.org/10.1021/acsaem.1c00455
ACS Appl. Energy Mater. 2021, 4, 4099−4111